AD-A190 915 DYNAMIC SHEAR BAND DEVELOPMENT IN PLANE STRAIN(U) BROWN 1/1
UNIV PROVIDENCE RI DIV OF ENGINEERING A NEEDLEMAN
NOV 87 7 ARO-22306.11-EG DAAG29-85-K-0003

UNCLASSIFIED F/G 20/11 NL

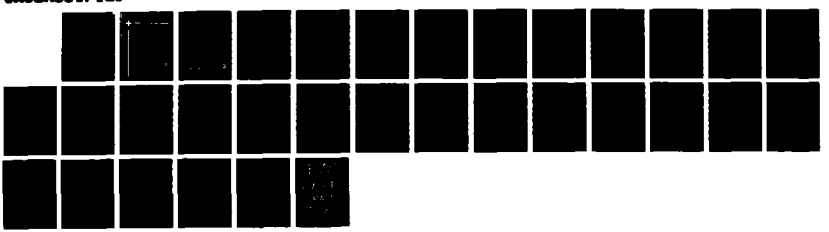

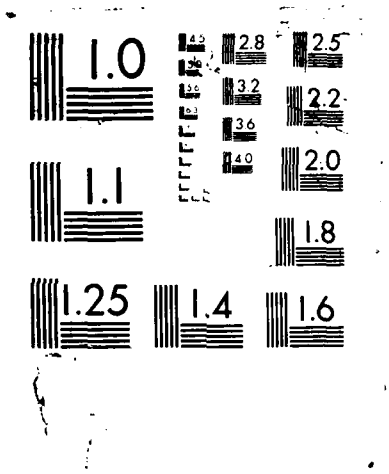
1.0
1.1
1.25
1.4
1.6
1.8
2.0
2.2
2.5
2.8
3.2
3.6
4.0

Brown University
DIVISION OF ENGINEERING
PROVIDENCE, R.I. 02912

Dynamic Shear Band Development in Plane Strain

by

A. Needleman
Division of Engineering
Brown University
Providence, RI 02912

Brown University
Division of Engineering
Providence, RI 02912

Dynamic Shear Band Development in Plane Strain

by

A. Needleman
Division of Engineering
Brown University
Providence, RI 02912

Brown University Technical Report
ARO Grant DAAG29-85-K-003
Report No. 7
November, 1987

UNCLASSIFIED

SECURITY CLASSIFICATION OF THIS PAGE (When Data Entered)

REPORT DOCUMENTATION PAGE		READ INSTRUCTIONS BEFORE COMPLETING FORM
1. REPORT NUMBER: ARO 22306.11-EG	2. GOVT ACCESSION NO.: N/A	3. RECIPIENT'S CATALOG NUMBER: N/A
4. TITLE (and Subtitle): "Dynamic Shear Band Development in Plane Strain"		5. TYPE OF REPORT & PERIOD COVERED
		6. PERFORMING ORG. REPORT NUMBER
7. AUTHOR(s): Alan Needleman		8. CONTRACT OR GRANT NUMBER(s): DAAG29-85-K-0003
9. PERFORMING ORGANIZATION NAME AND ADDRESS: Brown University, Box D, Division of Engineering, Providence, RI 02912		10. PROGRAM ELEMENT, PROJECT, TASK AREA & WORK UNIT NUMBERS: N/A
11. CONTROLLING OFFICE NAME AND ADDRESS: U.S. Army Research Office, P.O. Box 12211, Research Triangle Park, NC 27709		12. REPORT DATE
		13. NUMBER OF PAGES
14. MONITORING AGENCY NAME & ADDRESS (if different from Controlling Office)		15. SECURITY CLASS. (of this report): Unclassified
		15a. DECLASSIFICATION/DOWNGRADING SCHEDULE

16. DISTRIBUTION STATEMENT (of this Report)

Approved for public release; distribution unlimited.

17. DISTRIBUTION STATEMENT (of the abstract entered in Block 20, if different from Report)

N/A

18. SUPPLEMENTARY NOTES

The view, opinions, and/or findings contained in this report are those of the author and should not be construed as an official Department of the Army position, policy, or decision, unless so designated by other documentation.

19. KEY WORDS (Continue on reverse side if necessary and identify by block number)

20. ABSTRACT (Continue on reverse side if necessary and identify by block number)

Plane strain compression of a rectangular block is used as a model problem to investigate the dynamics of shear band development from an internal inhomogeneity. The material is characterized as a von Mises elastic-viscoplastic solid, with a hardness function that exhibits a local maximum. Regardless of whether the material is hardening or softening, plastic strain development involves the evolution of finger-like contours

DD FORM 1 JAN 73 1473 EDITION OF 1 NOV 65 IS OBSOLETE S/N 0102-014-6601

UNCLASSIFIED

SECURITY CLASSIFICATION OF THIS PAGE (When Data Entered)

Block 20 - Continuation of Abstract

emanating from the inhomogeneity at 45° to the compression axis. Once a given strain contour crosses the specimen, it fans out about its initial direction of propagation. For a softening solid, this fanning out ceases for some strain level greater than the strain at the hardness maximum and further straining takes place in an ever narrowing band. Many of the qualitative features of shear band development under dynamic loading conditions are the same as under quasi-static loading conditions, but a significant retardation of shear band development due to inertial effects is found.

1. Introduction

Large inelastic deformations are frequently accompanied by the formation of intense bands of localized shearing. Often the large localized strains in a shear band precipitate a shear fracture. In other circumstances shear bands do not lead to fracture but localized shearing becomes an important mechanism for subsequent plastic deformation. Hence shear bands have a dual significance; as a precursor to fracture and as a mechanism of large strain plastic response.

When the solid is considered to be deforming quasi-statically and isothermally, shear band localizations can be analyzed as a "material instability," within a framework due to Hadamard (1903), Thomas (1961), Hill (1962), Mandel (1966) and Rice (1977). Within this framework, a material element is considered subject to all around displacement boundary conditions consistent with homogeneous deformations; different homogeneous deformation states prevail outside and inside the band and the analysis determines the jumps in field quantities across the band interface. For rate independent solids, the onset of a shear band localization can occur as a bifurcation corresponding to a loss of ellipticity of the rate equilibrium equations, Hill (1962), Rice (1977). For rate sensitive solids a bifurcation is effectively excluded and the governing rate equations remain elliptic, although in the presence of initial band type imperfections shear band localizations do emerge, e.g. Pan et al. (1983).

The analysis of shear band development in non-homogeneously deforming solids requires a full boundary value problem solution. Such solutions have been obtained for the quasi-static development of shear bands, see e.g. Tvergaard et al. (1981), Triantafyllidis et al. (1982), LeMonds and Needleman (1986) and the review of Needleman and Tvergaard (1983), and have shown that shear bands do initiate with the orientation given by the "material instability" analysis. Shear band propagation, however, is greatly affected by the inhomogeneity of the surrounding fields.

The physical mechanisms responsible for triggering shear bands can vary widely. At low strain rates, a key feature of plastic material response for localization is the yield surface vertex structure implied by the discrete nature of crystallographic slip. The significance of a vertex lies in the reduced stiffness to a change in loading path which permits shear bands to emerge in strain hardening materials, see e.g. Rice (1977). At higher strain rates, thermal softening appears to play a major role in shear band formation, as originally suggested by Zener and Holloman (1944). An overview of conditions for high rate shear band formation in simple shear and correlation with experiments is given by Clifton et al. (1984).

Profusions of internal shear bands are sometimes observed, e.g. Anand and Spitzig (1980), and these bands appear to originate at internal inhomogeneities. Analyses of shear localization from internal strain concentrators have been carried out by Abeyaratne and Triantafyllidis (1981), Tvergaard (1982, 1987), Freund, Wu and Toulios (1985) and LeMonds and Needleman (1986).

Abeyaratne and Triantafyllidis (1981) investigated shear band initiation in quasi-statically deforming hypo-elastic and hyper-elastic solids in plane strain. LeMonds and Needleman (1986) also considered plane strain quasi-static deformations but analyzed the course of shear band development in elastic-viscoplastic solids, accounting for strain hardening, rate dependence, thermal softening and heat conduction. Tvergaard (1982, 1987) has studied the quasi-static response of porous plastic solids having two size scales of void nucleating particles and where early nucleation at relatively large particles triggers localization into a void sheet. In Freund, Wu and Toulios (1985) the dynamics of shear band propagation was analyzed for a nonlinear elastic solid in anti-plane strain.

Here, the dynamics of shear band development from internal material inhomogeneities under plane strain compressive loading is used as a model problem for investigating shear band propagation in a rate sensitive solid under plane strain conditions. The material is characterized as an elastic-viscoplastic von Mises solid. In order to simulate the phenomenon of thermal softening due to adiabatic heating, the material is taken to be strain softening. Although attention is focussed on circumstances where such softening is responsible for shear band development, it is important to emphasize that for more general constitutive descriptions of plastic flow, strain softening is not necessary to precipitate a shear band localization, Rudnicki and Rice (1975), Rice (1977). Due to the viscoplastic formulation wave speeds remain real even in the softening regime; in fact, regardless of the plastic pre-strain, wave speeds are set by the elastic moduli. Furthermore, as a consequence, the pathological mesh size effects encountered in localization analyses for rate independent solids are eliminated, Needleman (1987).

2. Problem Formulation

The analysis is based on a convected coordinate Lagrangian formulation of the field equations with the initial unstressed state taken as reference. All field quantities are considered to be functions of convected coordinates, y^i, which serve as particle labels, and time t. The position, relative to a fixed Cartesian frame, of a material point in the initial configuration is denoted by $\mathbf{x}$. In the current configuration the material point initially at $\mathbf{x}$ is at $\bar{\mathbf{x}}$. The displacement vector $\mathbf{u}$ and the deformation gradient $\mathbf{F}$ are defined by

$$\mathbf{u} = \bar{\mathbf{x}} - \mathbf{x} \quad , \qquad \mathbf{F} = \frac{\partial \bar{\mathbf{x}}}{\partial \mathbf{x}} \tag{2.1}$$

Base vectors in the reference configuration (unbarred) and in the current configuration (barred) are given by

$$\mathbf{g}_i = \frac{\partial \mathbf{x}}{\partial y^i} \quad , \qquad \bar{\mathbf{g}}_i = \frac{\partial \bar{\mathbf{x}}}{\partial y^i} \tag{2.2}$$

$$\mathbf{g}^i = g^{ij}\mathbf{g}_j\ , \qquad \bar{\mathbf{g}}^i = \bar{g}^{ij}\bar{\mathbf{g}}_j \tag{2.3}$$

where g^{ij} and $\bar{g}^{ij}$ are, respectively, the inverses of the metric tensors $g_{ij} = \mathbf{g}_i \cdot \mathbf{g}_j$ and $\bar{g}_{ij} = \bar{\mathbf{g}}_i \cdot \bar{\mathbf{g}}_j$.

The momentum balance can be expressed either in terms of the symmetric Cauchy stress tensor $\boldsymbol{\sigma}$ or the nonsymmetric nominal stress tensor $\mathbf{s}$. These are related to the force, $\mathbf{df}$, transmitted across a material element by

$$\mathbf{df} = \bar{\boldsymbol{\nu}} \cdot \boldsymbol{\sigma}\, \mathbf{d\bar{S}} = \boldsymbol{\nu} \cdot \mathbf{s}\, \mathbf{dS} \tag{2.4}$$

Here, $d\bar{S}$ and $\bar{\boldsymbol{\nu}}$ give the area and orientation, in the current configuration, of a material element that had area dS and orientation $\boldsymbol{\nu}$ in the reference configuration and the stress measures $\mathbf{s}$ and $\boldsymbol{\sigma}$ are related by

$$\mathbf{s} = \mathbf{F}^{-1} \cdot \boldsymbol{\tau} \qquad \boldsymbol{\tau} = \det(\mathbf{F})\boldsymbol{\sigma} \tag{2.5}$$

The dynamic principle of virtual work is written as

$$\int_V s^{ji}\delta F_{ij}\, dV = \int_S T^i \delta u_i\, dS - \int_V \rho \frac{\partial^2 u^i}{\partial t^2}\delta u_i\, dV \tag{2.6}$$

where V, S and ρ are the volume, surface and mass density, respectively, of the body in the reference configuration and

$$T^i = s^{ji}\nu_j \tag{2.7}$$

The specific problem considered is plane strain compression of an initially square block of dimension $2h_0 \times 2h_0$. The $y^1 - y^2$ plane is taken to be the plane of deformation and the compression axis is aligned with the y^2 direction. The origin of the coordinate system is placed at the center of the block and identical displacement histories are imposed at $y^2 = \pm h_0$ and the sides $y^1 = \pm h_0$ remain traction free. Attention is restricted to deformations that remain symmetric about both $y^1 = 0$ and $y^2 = 0$. The boundary conditions for the quadrant analyzed numerically are

$$\dot{u}_1 = 0 \qquad T^2 = 0 \qquad \text{at} \quad y^1 = 0 \tag{2.8}$$

$$\dot{u}_2 = 0 \qquad \dot{T}^1 = 0 \qquad \text{at} \quad y^2 = 0 \tag{2.9}$$

$$\dot{T}_1 = 0 \qquad \dot{T}^2 = 0 \qquad \text{at} \quad y^1 = h_0 \tag{2.10}$$

$$\dot{T}_1 = 0 \qquad \dot{u}^2 = \dot{U}(t) \qquad \text{at} \quad y^2 = h_0 \tag{2.11}$$

where $(\dot{})$ is $\partial(\ )/\partial t$.

The function $\dot{U}(t)$ in (2.10) is taken as

$$\dot{U}(t) = \begin{cases} V_1(t/t_1), & \text{for } t \le t_1; \\ V_1, & \text{for } t > t_1 \end{cases} \tag{2.12}$$

with V_1 being a prescribed velocity.

The material is characterized as an elastic-viscoplastic von Mises solid. The total rate of deformation, $\mathbf{D}$, is written as the sum of an elastic part, $\mathbf{D}^{\mathrm{e}}$, and a plastic part $\mathbf{D}^{\mathrm{p}}$, with

$$\mathbf{D}^{\mathrm{e}} = \frac{1+\nu}{E}\hat{\boldsymbol{\tau}} - \frac{\nu}{E}(\hat{\boldsymbol{\tau}} : \mathbf{I})\mathbf{I} \tag{2.13}$$

$$\mathbf{D}^{\mathrm{p}} = \frac{3\dot{\bar{\epsilon}}}{2\bar{\sigma}}\boldsymbol{\tau}' = \dot{\bar{\epsilon}}\mathbf{p} \tag{2.14}$$

where $\hat{\boldsymbol{\tau}}$ is the Jaumann rate of Kirchhoff stress, $\mathbf{I}$ is the identity tensor, $\hat{\boldsymbol{\tau}} : \mathbf{I}$ is the trace of $\hat{\boldsymbol{\tau}}$, $\dot{\bar{\epsilon}}$ is the effective plastic strain rate, E is Young's modulus, ν is Poisson's ratio and

$$\boldsymbol{\tau}' = \boldsymbol{\tau} - \frac{1}{3}(\boldsymbol{\tau} : \mathbf{I})\mathbf{I} \qquad \bar{\sigma}^2 = \frac{3}{2}\boldsymbol{\tau}' : \boldsymbol{\tau}' \tag{2.15}$$

Combining (2.13) and (2.14) and inverting to express $\hat{\boldsymbol{\tau}}$ in terms of $\mathbf{D}$ gives a relation of the form

$$\hat{\boldsymbol{\tau}} = \mathbf{L} : \mathbf{D} - \mathbf{P} \qquad \mathbf{P} = \dot{\bar{\epsilon}}\mathbf{L} : \mathbf{p} = \dot{\bar{\epsilon}}\mathbf{p} : \mathbf{L} \tag{2.16}$$

where $\mathbf{L}$ is the tensor of elastic moduli and the dyadic product $\mathbf{L} : \mathbf{p}$ denotes $L^{ijkl}p_{lk}$.

On the current base vectors (2.16) has the form

$$\mathring{\tau}^{ij} = L^{ijkl}\dot{E}_{lk} - P^{ij} \tag{2.17}$$

The Lagrangian strain rate appears in (2.17) via the identity $\dot{E}_{ij} = \bar{\mathbf{g}}_i \cdot \mathbf{D} \cdot \bar{\mathbf{g}}_j$ and its components on the reference base vectors are given by

$$\dot{E}_{ij} = \frac{1}{2}\left(F^k_{\cdot i}\dot{F}_{kj} + F^k_{\cdot j}\dot{F}_{ki}\right) \tag{2.18}$$

The constitutive relation (2.17) can be expressed in terms of the convected derivative of Kirchhoff stress on the current base vectors, i.e. $\mathring{\tau}^{ij} = \bar{\mathbf{g}}^i \cdot \mathring{\boldsymbol{\tau}} \cdot \bar{\mathbf{g}}^j$, as

$$\mathring{\tau}^{ij} = C^{ijkl}\dot{E}_{lk} - P^{ij} \tag{2.19}$$

where

$$C^{ijkl} = L^{ijkl} - \frac{1}{2}\left[\bar{g}^{ik}\tau^{jl} + \bar{g}^{il}\tau^{jk} + \bar{g}^{jk}\tau^{il} + \bar{g}^{jl}\tau^{ik}\right] \tag{2.20}$$

The uniaxial response is represented by the power law rate relation

$$\dot{\bar{\epsilon}} = \dot{\epsilon}_0[\bar{\sigma}/g(\bar{\epsilon})]^{1/m} \tag{2.21}$$

The hardness function $g(\bar{\epsilon})$, with $\bar{\epsilon} = \int \dot{\bar{\epsilon}}dt$, represents the effective stress versus effective strain response in a tensile test carried out at a strain-rate such that $\dot{\bar{\epsilon}} = \dot{\epsilon}_0$. In (2.21), σ_0 is a reference strength and $m > 0$ is the strain rate hardening exponent.

On quite general grounds, for metals undergoing plastic deformation due to dislocation motion, the plastic strain rate is appropriately taken as a function of the stress and the current state, Rice (1970). The relation (2.21) employs the idealization of a single parameter characterization of the current state. A fundamental distinction between rate dependent material behavior as embodied in (2.21) and rate independent behavior is that the plastic strain rate in (2.21) does not depend on incremental quantities. For structural metals at room temperature, values of m in the range 0.002 to 0.02 are representative; see, for example, data collected by Ghosh (1977). Even though there is no explicit plastic yielding condition in the constitutive formulation, for this range of m, there is an apparent rate dependent yield strength and an "unloading"-like response on strain rate reversal, see e.g. Needleman (1987).

The power law description of material strain rate sensitivity in (2.21) is not a fundamental physical relation, but it can provide a reasonable representation of the strain rate sensitivity of common structural metals over several decades of strain rate. The physical background for power law viscoplasticity, and its limitations, are discussed by Asaro (1983) and Klopp, Clifton and Shawki (1985).

The hardness function $g(\bar{\epsilon})$ is taken to have the form

$$g(\bar{\epsilon}) = \sigma_0 \frac{(1 + \bar{\epsilon}/\epsilon_0)^N}{1 + (\bar{\epsilon}/\epsilon_1)^2} \tag{2.22}$$

For $\epsilon_1 \to \infty$, (2.22) reduces to a power law hardening relation. As ϵ_1 decreases, $g(\bar{\epsilon})$ exhibits strain softening at decreasing values of $\bar{\epsilon}$. Figure 1 shows curves of $g(\bar{\epsilon})$ versus $\bar{\epsilon}$ with $N = 0.1$ and $\epsilon_0 = 0.00218$ and for $\epsilon_1 = 10^4 \times \epsilon_0$, $200 \times \epsilon_0$ and $100 \times \epsilon_0$. The finite element calculations to be discussed subsequently are based on the three hardness functions shown in Fig. 1.

Since the plastic strain rate in (2.21) depends on the current state and not on incremental quantities, the propagation of disturbances depends on the elastic stiffnesses, which is consistent with observation, see e.g. Clifton (1972). In particular, the speed at which incremental disturbances propagate does not depend explicitly on whether the material is hardening or softening. Over the range of stress and deformation states arising in the numerical examples here, the maximum $\| \boldsymbol{\tau} \| < 0.01 \times E$ and maximum principal logarithmic strains less than 0.5, wave speeds remain nearly constant at their linear elastic values, even in the softening regime.

3. Numerical Method

The discretization is carried out in the reference configuration with the convected coordinates, y^i, being the independent variables. Linear displacement triangular elements are used arranged in a quadrilateral pattern consisting of "crossed" triangles. The "crossed" triangular quadrilaterals are used both because of their ability to represent incompressible deformations without mesh locking, Nagtegaal et al. (1974), and because of their ability to reproduce localized deformation modes that are oblique to the quadrilateral mesh, Tvergaard et al. (1981), Needleman and Tvergaard (1983). A lumped mass matrix is used instead of the consistent mass matrix in (3.6), since this has been found preferable for explicit time integration procedures, from the point of view of accuracy as well as computational efficiency, Krieg and Key (1973). When the finite element approximations of the displacement components u^i are substituted into (2.6), and the integrations are carried out, the discretized equations of motion are obtained

$$\mathbf{M} \frac{\partial^2 \mathbf{U}}{\partial t^2} = \mathbf{R} \tag{3.1}$$

where $\mathbf{M}$ is a mass matrix, $\mathbf{U}$ is a nodal displacement vector and $\mathbf{R}$ is a nodal force vector.

An initial inhomogeneity is specified that corresponds to a local reduction in flow strength, σ_0 in (2.11) of the form

$$\sigma_0(y^1, y^2) = \bar{\sigma}_0 \left[1 - \alpha \exp\{[(y^1 - y_0^1)^2 + (y^2 - y_0^2)^2]/r_0^2\} \right] \tag{3.2}$$

where y_0^1 and y_0^2 specify the location of the inhomogeneity and r_0 and α give the inhomogeneity size and magnitude, respectively.

At $t = 0$, the rectangular block under consideration is taken to be stress free and motionless. The equations of motion (3.1) are integrated using a central difference scheme that can be regarded as a member of the Newmark family of time stepping algorithms, Hughes and Belytschko (1983). At each time increment the stress state is updated using the rate tangent method of Peirce et al. (1984). This combination of a central difference time stepping scheme in conjunction with the tangent modulus stress updating algorithm is discussed by Moran (1987) and has also been used in Needleman (1987) and Tvergaard and Needleman (1987). For the present problem, the basic equations take the form

$$\mathbf{U}_{n+1} = \mathbf{U}_n + \Delta t \mathbf{V}_n + \frac{1}{2}(\Delta t)^2 \frac{\partial \mathbf{V}_n}{\partial t} \tag{3.3}$$

$$\frac{\partial \mathbf{V}_{n+1}}{\partial t} = -\mathbf{M}^{-1}\mathbf{R}_{n+1} \tag{3.4}$$

$$\mathbf{V}_{n+1} = \mathbf{V}_n + \frac{1}{2}\Delta t \left[\frac{\partial \mathbf{V}_n}{\partial t} + \frac{\partial \mathbf{V}_{n+1}}{\partial t} \right] \tag{3.5}$$

Here, $\mathbf{V}$ is the vector of nodal displacement and velocity, $\mathbf{M}^{-1}$ denotes the inverse of the mass matrix and the subscripts n and $n+1$ refer to quantities evaluated at t_n and t_{n+1}, respectively.

At each integration point, the stress tensor is updated via

$$\tau_{n+1}^{ij} = \tau_n^{ij} + \Delta t \dot{\tau}^{ij} \tag{3.6}$$

The stress rate components, $\dot{\tau}^{ij}$, are computed from (2.19) and (2.20) with $\mathbf{L}$ and $\mathbf{P}$ replaced by the corresponding rate tangent quantities.

$$\mathbf{L}^{tan} = \mathbf{L} - \frac{\xi}{1+\xi}\frac{1}{h}(\mathbf{L}:\mathbf{p}) \otimes (\mathbf{L}:\mathbf{p}) \qquad \mathbf{P}^{tan} = \frac{\dot{\bar{\epsilon}}_t}{1+\xi}\mathbf{L}:\mathbf{p} \tag{3.7}$$

where $\mathbf{A} \otimes \mathbf{B}$ denotes the tensor product $A^{ij}B^{kl}$ and

$$\dot{\bar{\epsilon}}_t = \dot{\epsilon}_0[\bar{\sigma}/g(\bar{\epsilon})]^{1/m} \qquad \xi = (\theta\Delta t)h\frac{\partial\dot{\bar{\epsilon}}}{\partial\bar{\sigma}} \tag{3.8}$$

$$h = \mathbf{p}:\mathbf{L}:\mathbf{p} - \left(\frac{\partial\dot{\bar{\epsilon}}}{\partial\bar{\epsilon}}\right)\left(\frac{\partial\dot{\bar{\epsilon}}}{\partial\bar{\sigma}}\right)^{-1} \tag{3.9}$$

In the second of (3.8), θ is a parameter of the integration scheme that is taken to be unity in the numerical calculations here.

The effective plastic strain is updated using $\bar{\epsilon}_{n+1} = \bar{\epsilon}_n + \Delta t\dot{\bar{\epsilon}}$ with

$$\dot{\bar{\epsilon}} = \frac{\Delta\bar{\epsilon}}{\Delta t} = \frac{\dot{\bar{\epsilon}}_t}{1+\xi} + \frac{\xi}{(1+\xi)h}(\mathbf{L}:\mathbf{p}):\mathbf{D} \tag{3.10}$$

The constitutive updating calculations use $(\mathbf{U}_{n+1} - \mathbf{U}_n)/\Delta t$ to represent the displacement rate components in (2.18).

In the limit $\xi \to \infty$, (3.7) through (3.10) reduce to their rate independent counterparts. On the other hand, for $\xi = 0$, which results from setting $\theta = 0$ in the second of (3.8), the Euler integration scheme is recovered.

4. Results

In the calculations here, all material parameters are kept fixed except for ϵ_1 which governs the rate of softening. Although the aim here is not to model any particular material, the fixed property values are taken to be representative of structural steels: $E = 211$ GPa, $\sigma_0 = 460$ MPa, $\epsilon_0 = \sigma_0/E = 0.00218$, $\nu = 0.3$, $N = 0.1$, $m = 0.01$ and $\dot{\epsilon}_0 = 0.002$ sec^{-1}. The initial inhomogeneity in (3.2) is specified by $y_0^1 = y_0^2 = 0$, $\alpha = 0.2$ and $r_0 = 0.1$ mm. With $\rho = 7800$ kg/m^3 $= 7.8 \times 10^{-3}$MPa/(m/sec)^2, the elastic wave speeds are

$$c_0 = \sqrt{\frac{2G}{\rho}} = 3.23 \times 10^3\text{m/sec} \qquad c_1 = \sqrt{\frac{2G(1-\nu)/(1-2\nu)}{\rho}} = 6.03 \times 10^3\text{m/sec} \tag{4.1}$$

where $2G = E/(1+\nu)$.

Three values of the imposed velocity are considered; $V_1 = -3$ m/sec, $V_1 = -10$ m/sec and $V_1 = -30$ m/sec, which correspond to $| V_1 | /c_0 = 0.929 \times 10^{-3}$, $| V_1 | /c_0 = 3.10 \times 10^{-3}$ and $| V_1 | /c_0 = 9.29 \times 10^{-3}$, respectively. In each case the rise time, t_1 in (2.12), is 0.1×10^{-6} sec. Also, the block size h_0 is taken to be 1 mm, so that the nominal strain rates for the three imposed velocities are 3×10^3, 10^4 and 3×10^4, respectively.

A uniform finite element mesh is used, with the elements arranged so that at a strain a little larger than when the peak hardness is attained, the element diagonals are oriented for 45° shear bands. For the majority of calculations, with $\epsilon_1 = 200 \times \epsilon_0$, a 26×20 element mesh is used (the deformed mesh is shown subsequently in Fig. 8), while with $\epsilon_1 = 100 \times \epsilon_0$ a 24×20 mesh is used. In each case the 20 element division is in the y^2 direction. A variable time step method is used with one criterion limiting the time step being the requirement that the time step be no greater than the time for a wave travelling at velocity c_1 to traverse half the smallest element side. With the ratio of wave speeds in (4.1), this is about 94% of the time for a wave travelling at the shear wave speed c_0 to traverse the smallest element side. Other time step limits are set by stability requirements for the rate tangent modulus integration of the constitutive relations. However, in the problems considered here these are rarely operative and the time step limits set by stability requirements for the explicit integration of the equations of motion determine the maximum permissible time step.

Figure 2 shows curves of average stress versus end displacement, with an imposed velocity of 10 m/sec, for each of the hardening relations in Fig. 1. The average stress (per unit out-of-plane thickness) is given by

$$\sigma_{ave} = \frac{1}{h} \int_0^{h_0} [T^1]_{y^2 = h_0} dy^1 \tag{4.2}$$

where h is the current width at $y^2 = h_0$ and the end displacement is $U_1 = \int_0^t V_1 dt$.

The initial response is identical for the three hardening relations. Once extensive plastic deformation occurs, dynamic effects are rapidly damped. For the softening solids there is an abrupt stress drop that is associated with shear band formation.

Before considering shear band propagation, the dynamics of strain development for the hardening solid is shown in Fig. 3. Strain contours originate at the inhomogeneity and evolve as finger-like contours at 45° to the compression axis. Once a given contour crosses the specimen, it fans out about its initial direction of propagation. In Fig. 3, the propagation speed along the 45° direction is 830 m/sec for the 0.05 contour and 1100 m/sec for the 0.09 contour.

For the softening solid in Fig. 4, strain development initially follows the pattern shown in Fig. 3. A shear band bifurcation occurs for the underlying rate independent solid at the attainment of

the maximum hardness and the 45° shear band orientation is the most critical one. Eventually, for a strain level beyond the peak in Fig. 1, spreading in the direction perpendicular to the initial propagation direction slows down and further straining occurs in a band. The ultimate course of events is essentially determined at the stage of loading shown in Fig. 4b; continually increasing strain in a shear band with very little change in strain outside the band. Between Figs. 4a and 4b the speeds of propagation of the 0.07 and 0.08 contours are 2200 m/sec and 1600 m/sec, respectively. Between Figs. 4b and 4c, the propagation speed of the 0.09 contour along the band is 2900 m/sec, which is approaching the shear wave speed. For the case in Fig. 2 with $\epsilon_1 = 200 \times \epsilon_0$, plastic strain contour speeds at a similar stage of band development are somewhat slower, around 1300 m/sec.

Figure 5 shows the effect of prescribed velocity on the average stress versus end displacement response for a material characterized by the hardness function with $\epsilon_1 = 200 \times \epsilon_0$. With $V_1 = -3$ m/sec, corresponding to an average strain rate of 3000/sec, the response is essentially quasi-static as soon as there is any significant plasticity. When the velocity is increased to -10 m/sec, (this is the same case as B in Fig. 2) dynamic effects persist much longer, but have been essentially damped out by the time localization initiates. At $V_1 = -30$ m/sec, significant inertial effects are evident through localization initiation. If the imposed velocity were increased much beyond -30 m/sec, the average stress would change sign at the first trough, indicating a separation event, subsequent to which imposition of (2.11) would not be the physically appropriate boundary condition.

Quasi-static calculations were carried out using the same material properties and using an identical finite element mesh for the cases in Fig. 5 with $V_1 = -3$ m/sec and $V_1 = -30$ m/sec. With $V_1 = -3$ m/sec, except for the lack of "wiggles," the quasi-statically computed stress strain curve coincides with that in Fig. 5 up to the drop due to shear localization. The quasi-static calculation gives localization at a strain 0.0006 smaller than given by the dynamic calculation in Fig. 5, but other than this small shift, the quasi-static post-localization response is indistinguishable from the dynamic response shown. The case analyzed here is one for which there are equilibrium solutions with increasing end displacement during shear band development. In some circumstances, see e.g. Tvergaard et al. (1981), there may be no equilibrium solutions having increasing end displacement as localization proceeds and in such cases dynamic effects may be significant for localization development even at very low imposed velocities.

In the quasi-static analysis with a prescribed velocity of -30 m/sec, the order of magnitude increase in the nominal applied strain rate, from 3×10^3 to 3×10^4, gives an increase in stress level of about 2% ($10^{0.01} \approx 1.02$), but shear localization, as signalled by the drop in the overall stress-strain curve, occurs at nearly the same end displacement value as with $V_1 = -3$ m/sec. This behavior is expected, since analyses of the effect of rate sensitivity on plastic instabilities

in rigid-plastic power law rate hardening materials, e.g. Hutchinson and Neale (1977), show that while the instability strain depends sensitively on the strain rate hardening exponent, it is independent of the rate. Hence, the delay in shear band initiation with increasing imposed velocity evident in Fig. 5 is a consequence of material inertia and not of material strain rate sensitivity.

There is a significant distinction between the dynamic and quasi-static formulations regarding characteristic time scales. In the quasi-static formulation there is a single material time scale, $1/\dot{\epsilon}_0$, while in the dynamic formulation there are two; $1/\dot{\epsilon}_0$ and a problem dependent time scale that is a wave speed divided by a characteristic length, e.g. c_0/h_0. The rate of strain development scales with $V_1/\dot{\epsilon}_0 h_0$ in the quasi-static formulation, but not in the dynamic analyses, due to inertial effects.

Figures 6 and 7 show the course of shear band development for $V_1 = -3$ m/sec and $V_1 = -30$ m/sec, respectively. There is a clear effect of imposed velocity on the speed of propagation of the strain contours. For example, in Fig. 6 the 0.15 contour propagates along the band at a speed between 590 m/sec and 680 m/sec, while in Fig. 7 the corresponding propagation speed is 2500 m/sec. The qualitative features of shear band development do not depend on the imposed rate, but it is evident in Figs. 6 and 7, as well as in Fig. 5, that there is a delay in shear band initiation with increasing rate.

Figure 8 shows deformed finite element meshes at two stages of deformation. Fig. 8a corresponds to the stage of deformation in Fig. 7c. Even though the shear band has already formed, this is difficult to ascertain from the deformed mesh. At the stage of deformation in Fig. 8b, the mesh is incapable of resolving the sharp strain gradients across the band and the discreteness of the mesh significantly affects the computed response. This figure is included to illustrate the ability of the mesh to develop a narrow shear band, which confirms, for example, that the initial thickness of the band evident in Figs. 3, 4, 6 and 7 is an actual reflection of the inhomogeneity size and is not a mesh artifact.

In order to explore the effect of mesh on the computed response, two additional meshes were used for the case with $V_1 = -10$ m/sec and $\epsilon_1 = 100 \times \epsilon_0$. In one case the mesh aspect ratio was varied, while in the other case the aspect ratio was kept fixed, but a finer mesh was used. The computed average stress versus end-displacement curves are shown in Fig. 9. In the 29×20 mesh the band is spread across two rows of quadrilaterals. This gives rise to a significant mesh induced delay in the onset of shear band formation even though this mesh has more elements than the reference mesh. Increasing the number of elements, but keeping a fixed aspect ratio leads to a slightly earlier onset of localization, which is in part due to a better resolution of the strain concentration at the inhomogeneity. The finer mesh can also resolve larger gradients and so exhibits a greater stress drop before mesh induced stiffening occurs. The post-localization

rise in the stress versus end-displacement curve for the 29 x 20 mesh is a consequence of mesh induced stiffening when gradients in the band become very large. A similar stiffening occurs for the other two meshes in Fig. 9, but occurs later in the deformation history with improved resolution of the band.

The speed of propagation of the constant plastic strain contours does not differ much between these three meshes. For the 24 x 20 mesh in Fig. 4, the propagation speed along the band of the 0.08 plastic strain contour is 1600 m/sec. At a similar stage of deformation with the 36 x 30 mesh the 0.08 contour is propagating at 1900 m/sec and at 1600 m/sec with 29 x 20 mesh. The difference in propagation speed found for the 36 x 30 mesh is attributable more to variations in speed as the contour propagates along the band than to the increased resolution; with the 24 x 20 mesh in Fig. 4, a propagation speed of 2200 m/sec is found for the 0.07 contour.

5. Discussion

Key features of the phenomenology of shear band development under dynamic loading conditions are the same as under quasi-static loading conditions. Shear bands develop at 45° from the compression axis, as expected based on a quasi-static "material instability" analysis. Under quasi-static loading conditions, for the viscoplastic solids considered here, the strain at which shear bands initiate is an outcome of the competition between the destabilizing influence of the inhomogeneity and the stabilizing effect of material strain rate sensitivity. Under dynamic loading conditions, a delay in shear band development arises due to inertial effects. Also, since dynamic effects induce non-homogeneous deformations, an inhomogeneity is not required to initiate localization but, in the circumstances analyzed here, the inhomogeneity plays the major role in triggering the onset of shear localization.

The key to the development of shear bands in the calculations here is the speed of propagation of plastic strain contours in the direction normal to the eventual band. This is consistent with what would be expected based on a rate independent shear band bifurcation analysis, where, at bifurcation, the propagation velocity of shear waves normal to the band vanishes. The vanishing of this wave speed is also the shear band initiation criterion that emerges from the perturbation analysis of Freund, Wu and Toulios (1985). The process of band formation, a cascade of finger-like plastic strain contours emanating from the inhomogeneity and from a small region where the band intersects the impacted surface, in a continually sharpening band, is one that makes defining a band propagation speed somewhat arbitrary. Although there is no single event that can be identified with shear band initiation, there is a reasonably well identifiable strain in Figs. 4, 6 and 7 above which all further straining occurs within a narrowing band. A band propagation speed can be identified with the propagation speed of some particular strain contour along the band, but this speed is not associated with some sharp gradient propagating through the material.

The main strain gradients occur across the band and large strain gradients do not develop along most of the band; substantial strain gradients in the band direction are confined to very near the inhomogeneity and to a small region where the band intersects the impacted surface. This can be seen in Figs. 4, 6, and 7; for example, even in Fig. 7c, the element in the center of the inhomogeneity has an effective plastic strain of 0.33, while in the adjacent element in the shear band the effective plastic strain value is 0.25 (clearly, the mesh used here does not resolve the details of field distributions around the inhomogeneity). The continually steepening strain gradient across the band is much like that in one dimensional simple shear calculations, e.g. Wada et al. (1978), Wu and Freund (1984), Shawki, Clifton and Majda (1987) and Needleman (1987). Such narrowing shear bands are observed, Marchand and Duffy (1987). In actuality, of course, under the conditions of temperature, strain and strain rate that prevail in a narrow shear band, material behavior is not described by the sort of simple phenomenological constitutive relation used in this investigation. Also, some material dependent length scale ultimately sets a minimum band thickness.

The situation analyzed in this investigation is one where, just prior to shear band formation, the stress and deformation fields are rather uniform. When shear band development takes place from a more non-uniform deformation state, the gradients in the background field retard shear band growth, as is shown in quasi-static analyses, Tvergaard et al. (1981) and Triantafyllidis et al. (1982). Under dynamic loading conditions, when there are strong unfavorable gradients, shear bands are likely to propagate in a more crack-like fashion than in the cases analyzed here.

A strain softening constitutive relation has been used as a simple model for a thermal softening solid. For an actual thermal softening solid, since the softening behavior is governed by the current rate of plastic dissipation, increased softening would accompany an increase in imposed strain rate and this would tend to counteract the delay in localization due to inertial effects.

Acknowledgements

The support of this work through ARO Grant DAAG29-85-K-0003 is gratefully acknowledged. The computations reported on here were carried out on an Alliant FX-8 computer at the Brown University, Division of Engineering, Computational Mechanics Facility. I am pleased to acknowledge helpful discussions with Professor R.J. Clifton of Brown University.

References

Abeyaratne, R. and Triantafyllidis, N., 1981, "The Emergence of Shear Bands in Plane Strain," *Int. J. Solids Struct.*, Vol. 17, pp. 1113-1134.

Anand, L. and Spitzig, W.A., 1980, "Initiation of Localized Shear Bands in Plane Strain," *J. Mech. Phys. Solids*, Vol. 28, pp. 113-128.

Asaro, R.J., 1983, "Mechanics of Crystals and Polycrystals," *Adv. Appl. Mech.*, Vol. 23, pp. 2-115.

Clifton, R.J., 1972, "Plastic Waves: Theory and Experiment," Mechanics Today, Vol. 1, (ed. S. Nemat-Nasser), Pergamon Press, Oxford, pp. 102-167.

Clifton, R.J., Duffy, J., Hartley, K.A. and Shawki, T.G., 1984, "On Critical Conditions for Shear Band Formation at High Rates," *Scripta Metall.*, Vol. 18, pp. 443-448.

Freund, L.B., Wu, F.H. and Toulios, M., 1985, "Initiation and Propagation of Shear Bands in Antiplane Shear Deformation," Proc. Considère Memorial Symposium, (ed. J. Salençon), Ecole Nationale des Ponts et Chaussées, Paris, pp. 125-134.

Ghosh, A.K., 1977, "The Influence of Strain Hardening and Strain–Rate Sensitivity on Sheet Metal Forming," *J. Eng. Matl. Tech.*, Vol. 99, pp. 264-274.

Hadamard, J.J., 1903, Leçons sur la Propagation des Ondes et les Équations de L'Hydrodynamique. Libraire Scientifique A. Hermann, Paris.

Hill, R., 1962, "Acceleration Waves in Solids," *J. Mech. Phys. Solids*, Vol. 10, pp. 1-16.

Hughes, T.J.R. and Belytschko, T., 1983, "A Precis of Developments in Computational Methods for Transient Analysis," *J. Appl. Mech.*, Vol. 50, pp. 1033-1041.

Hutchinson, J.W. and Neale, K.W., 1977, "Influence of Strain Rate Sensitivity on Necking under Uniaxial Tension," *Acta Met.*, Vol. 25, pp. 839-846.

Klopp, R.W., Clifton, R.J. and Shawki, T.G., 1985, "Pressure-Shear Impact and the Dynamic Viscoplastic Response of Metals," *Mech. Matl.*, 4, pp. 375-385.

Krieg, R.D. and Key, S.W., 1973, "Transient Shell Response by Numerical Time Integration," *Int. J. Numer. Meth. Engng.*, Vol. 7, pp. 273-286.

LeMonds, J. and Needleman, A., 1986, "Finite Element Analysis of Shear Localization in Rate and Temperature Dependent Solids," *Mech. Matl.*, 5, pp. 339-361.

Mandel, J., 1966, "Conditions de Stabilité et Postulat de Drucker," Rheology and Soil Mechanics, (ed. by J. Krautchenko and P.M. Sirieys), Springer-Verlag, Berlin, pp. 58-68.

Marchand, A. and Duffy, J., 1987, "An Experimental Study of the Formation Process of Adiabatic Shear Bands in a Structural Steel," *J. Mech. Phys. Solids*, in press.

Moran, B., 1987, "A Finite Element Formulation for Transient Analysis of Viscoplastic Solids with Application to Stress Wave Propagation Problems," *Comp. Struct.*, Vol. 27, pp. 241-247.

Nagtegaal, J.C., Parks, D.M. and Rice, J.R., 1974, "On Numerically Accurate Finite Element Solutions in the Fully Plastic Range," *Comp. Meth. Appl. Mech. Eng.*, Vol. 4, pp. 153-177.

Needleman, A., 1987, "Material Rate Dependence and Mesh Sensitivity in Localization Problems," *Comp. Meth. Appl. Mech. Eng.*, in press.

Needleman, A. and Tvergaard, V., 1983, "Finite Element Analysis of Localization in Plasticity," Finite Elements–Special Problems in Solid Mechanics, Vol. 5, (ed. J.T. Oden and G.F. Carey), Prentice-Hall, Englewood Cliffs NJ, pp. 94-157.

Pan, J. Saje, M. and Needleman, A., 1983, "Localization of Deformation in Rate Sensitive Porous Plastic Solids," *Int. J. Fracture*, Vol. 21, pp. 261-278.

Peirce, D., Shih, C.F.,and Needleman, A., 1984, "A Tangent Modulus Method for Rate Dependent Solids," *Comp. Struct.* Vol. 18, pp. 875-887.

Rice, J.R., 1970, "On the Structure of Stress-Strain Relations for Time-Dependent Plastic Deformation in Metals," *J. Appl. Mech.*, Vol. 37, pp. 728-737.

Rice, J.R., 1977, "The Localization of Plastic Deformation," Theoretical and Applied Mechanics, Proc. 14th Int. Congr. Theoret. Appl. Mech. (ed. W.T. Koiter), North-Holland, Amsterdam, pp. 207-220.

Rudnicki, J.W. and Rice, J.R., 1975, "Conditions for the Localization of Deformation in Pressure-Sensitive Dilatant Materials," *J. Mech. Phys. Solids*, Vol. 23, pp. 371-394.

Shawki, T.G., Clifton, R.J. and Majda, G., 1987, "Shear Band Formation in Thermal Viscoplastic Materials," to be published.

Thomas, T.Y., 1961, "Plastic Flow and Fracture of Solids," Academic Press, New York.

Triantafyllidis, N., Needleman, A. and Tvergaard, V., 1982, "On the Development of Shear Bands in Pure Bending," *Int. J. Solids Struct.*, Vol. 18, pp. 121-138.

Tvergaard, V., 1982, "Ductile Fracture by Cavity Nucleation Between Larger Voids," *J. Mech.*

Phys. Solids, Vol. 30, pp. 265-286.

Tvergaard, V., 1987, "Effect of Anisotropic Hardening on Ductile Failure of a Material Containing Two Size-Scales of Particles," DCAMM Report 354, The Technical University of Denmark.

Tvergaard, V., and Needleman, A., 1987, "Temperature and Rate Dependence of Charpy V-Notch Energies for a High Nitrogen Steel," to be published.

Tvergaard, V., Needleman, A. and Lo, K.K., 1981, "Flow Localization in the Plane Strain Tensile Test," *J. Mech. Phys. Solids*, Vol. 29, pp. 115-142.

Wada, M., Nakamura, T. and Kinoshita, N., 1978, "Distribution of Temperature, Strain Rate and Strain in Plastically Deforming Metals at High Strain Rates," *Phil. Mag. A*, Vol. 38, pp. 167-185.

Wu, F.H. and Freund, L.B., 1984, "Deformation Trapping due to Thermoplastic Instability in One-Dimensional Wave Propagation," *J. Mech. Phys. Solids*, Vol. 32, pp. 119-132.

Zener, C. and Holloman, J.H., 1944, "Effect of Strain Rate upon Plastic Flow of Steel," *J. Appl. Phys.*, Vol. 15, pp. 22-32.

Figure Captions

Figure 1 Curves of hardness g versus effective plastic strain, ϵ, from (2.22) with $N = 0.1$, $\epsilon_0 = 0.00218$ and (A) $\epsilon_1 = 10^4 \times \epsilon_0$, (B) $\epsilon_1 = 200 \times \epsilon_0$ and (C) $\epsilon_1 = 100 \times \epsilon_0$.

Figure 2 Average stress versus end displacement curves with a prescribed velocity of $V_1 = -10$ m/sec. The fixed material properties and initial inhomogeneity are specified in the text and curves (A), (B) and (C) correspond to the three hardness functions shown in Fig. 1.

Figure 3 Contours of constant effective plastic strain, ϵ, for a hardening solid, $\epsilon_1 = 10^4 \times \epsilon_0$. The fixed material properties and initial inhomogeneity are specified in the text and the prescribed end velocity is $V_1 = -10$ m/sec; (a) $t = 6.44 \times 10^{-6}$ sec (b) $t = 6.71 \times 10^{-6}$ sec (c) $t = 6.98 \times 10^{-6}$ sec (d) $t = 7.25 \times 10^{-6}$ sec.

Figure 4 Contours of constant effective plastic strain, ϵ, for a softening solid, $\epsilon_1 = 100 \times \epsilon_0$. The fixed material properties and initial inhomogeneity are specified in the text and the prescribed end velocity is $V_1 = -10$ m/sec; (a) $t = 4.75 \times 10^{-6}$ sec (b) $t = 5.02 \times 10^{-6}$ sec (c) $t = 5.28 \times 10^{-6}$ sec.

Figure 5 Average stress versus end displacement curves for a softening solid, $\epsilon_1 = 200 \times \epsilon_0$ with (A) $V_1 = -30$ m/sec (B) $V_1 = -10$ m/sec and (C) $V_1 = -3$ m/sec.

Figure 6 Contours of constant effective plastic strain, ϵ, for a softening solid, $\epsilon_1 = 200 \times \epsilon_0$. The fixed material properties and initial inhomogeneity are specified in the text and the prescribed end velocity is $V_1 = -3$ m/sec; (a) $t = 28.67 \times 10^{-6}$ sec (b) $t = 29.19 \times 10^{-6}$ sec (c) $t = 29.71 \times 10^{-6}$ sec.

Figure 7 Contours of constant effective plastic strain, ϵ, for a softening solid, $\epsilon_1 = 200 \times \epsilon_0$. The fixed material properties and initial inhomogeneity are specified in the text and the prescribed end velocity is $V_1 = -30$ m/sec; (a) $t = 3.24 \times 10^{-6}$ sec (b) $t = 3.50 \times 10^{-6}$ sec (c) $t = 3.76 \times 10^{-6}$ sec.

Figure 8 Deformed finite element meshes for a softening solid, $\epsilon_1 = 200 \times \epsilon_0$. Each quadrilateral consists of four "crossed" triangular elements. The fixed material properties and initial inhomogeneity are specified in the text and the prescribed end velocity is $V_1 = -30$ m/sec; (a) $t = 3.76 \times 10^{-6}$ sec (b) $t = 4.79 \times 10^{-6}$ sec.

Figure 9 Stress versus end displacement for a softening solid, $\epsilon_1 = 200 \times \epsilon_0$, with a prescribed velocity $V_1 = -10$ m/sec using three meshes; (A) 29×20 (B) 21×20 and (C) 36×30.

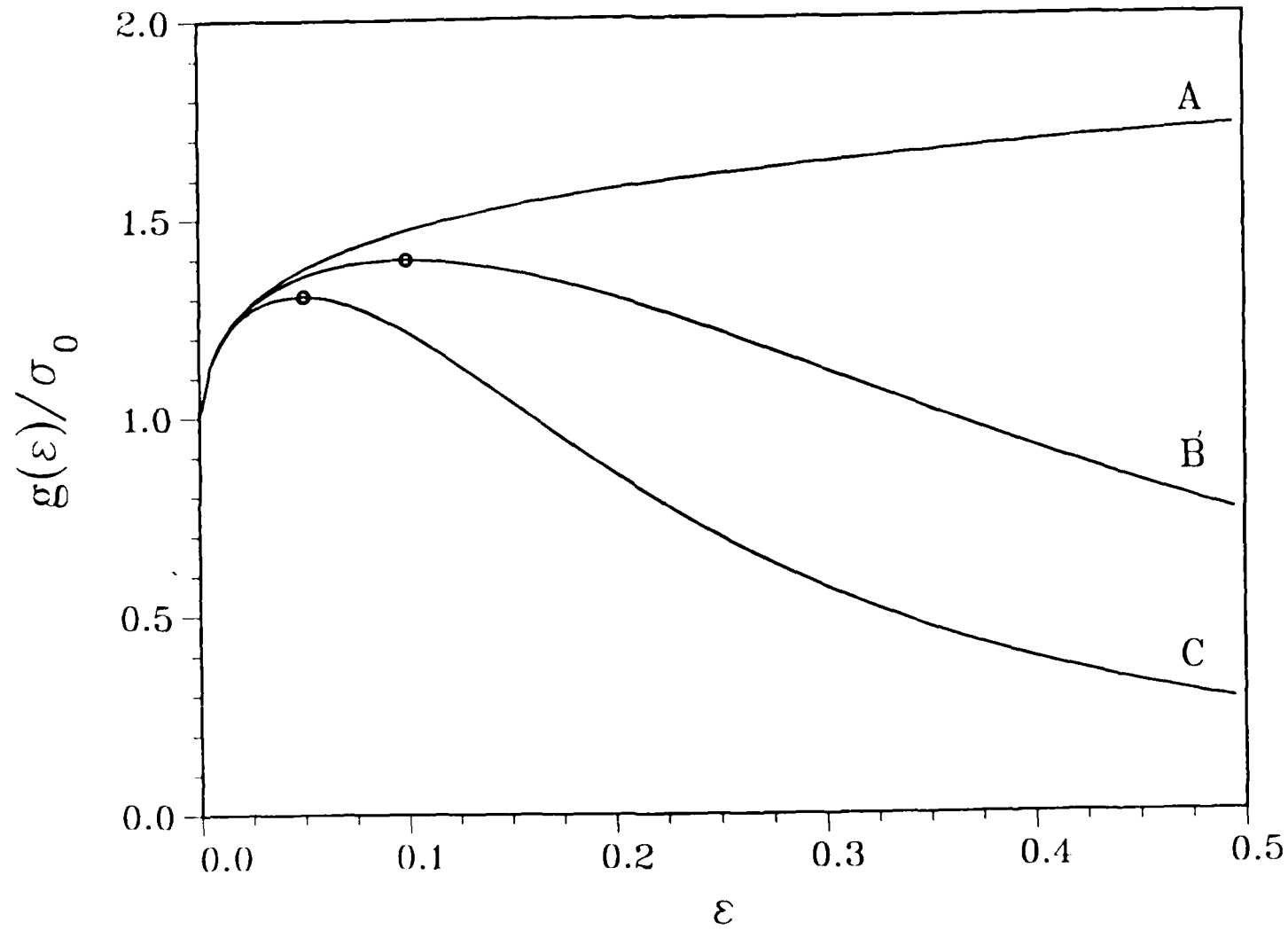
2.0
1.5
1.0
0.5
0.0
$g(\varepsilon)/\sigma_0$
A
B
C
0.0
0.1
0.2
0.3
0.4
0.5
ε

Figure 1

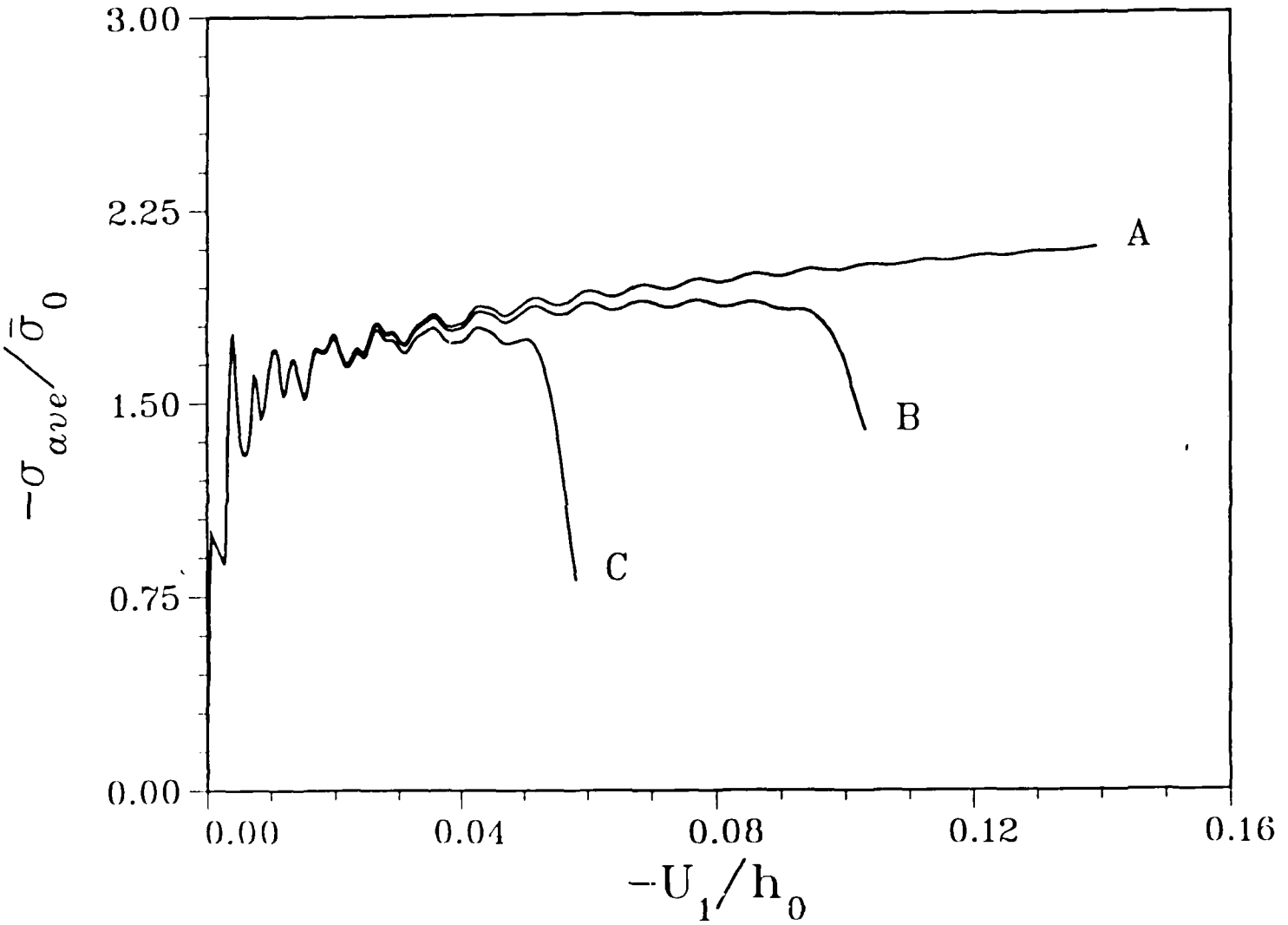
3.00
2.25
1.50
0.75
0.00
$-\sigma_{ave}/\bar{\sigma}_0$
A
B
C
0.00
0.04
0.08
0.12
0.16
$-U_1/h_0$

Figure 2

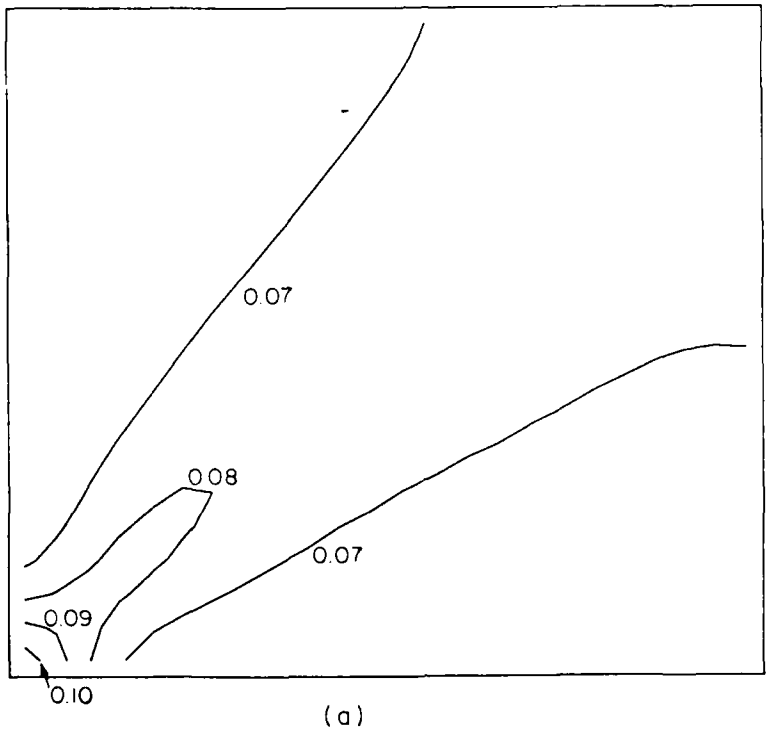

(a)

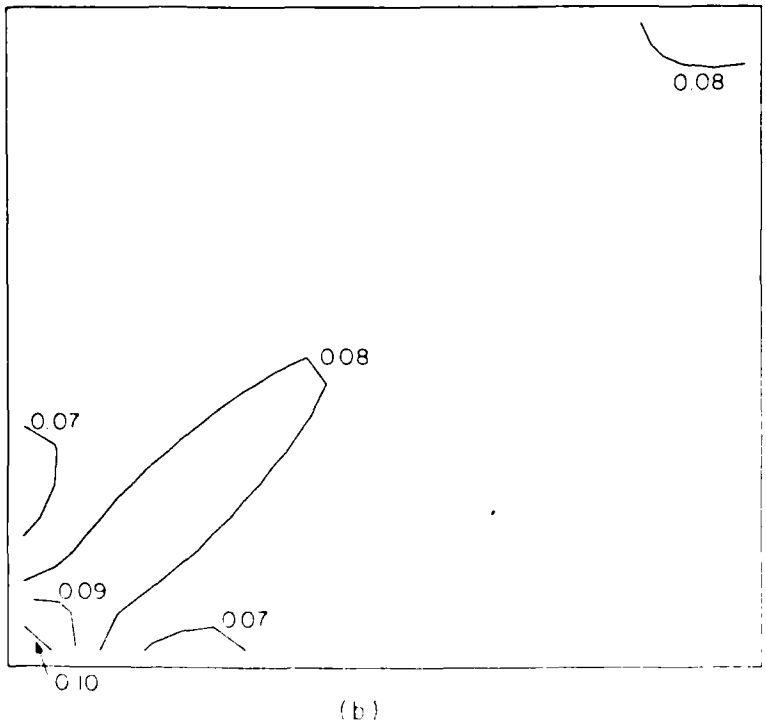

(b)

Figure 3

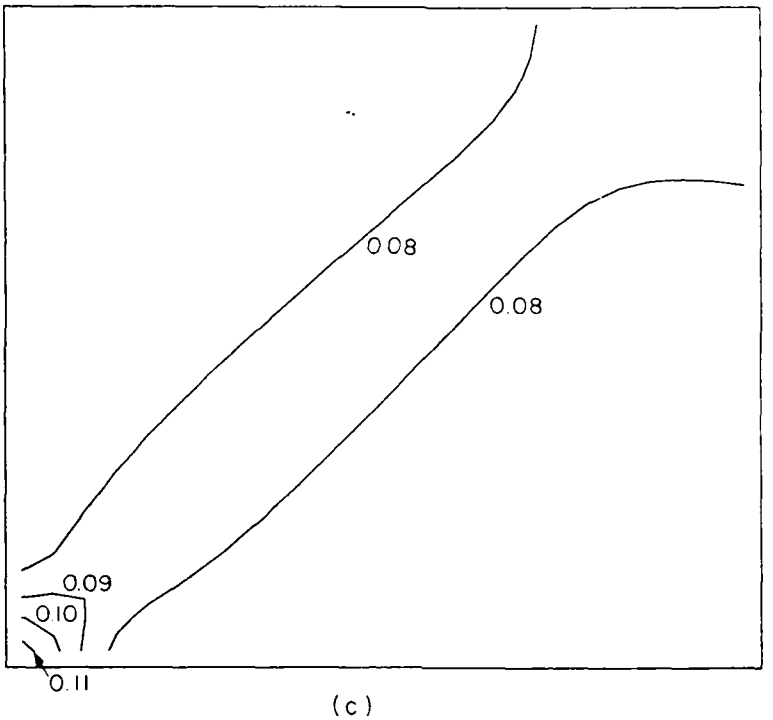

(c)

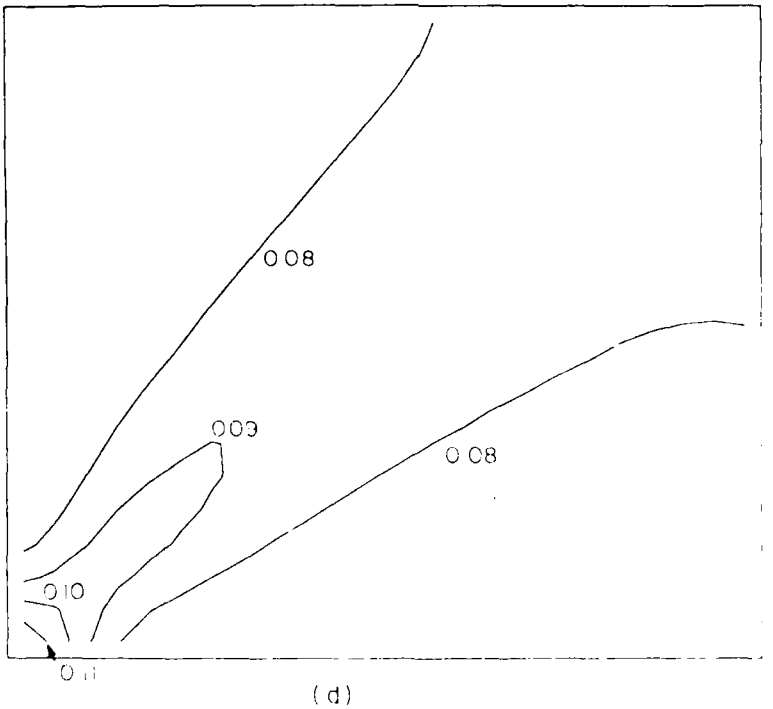

(d)

Figure 3 (Cont'd)

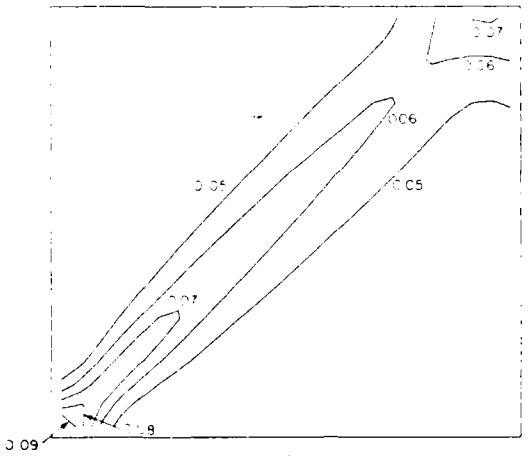

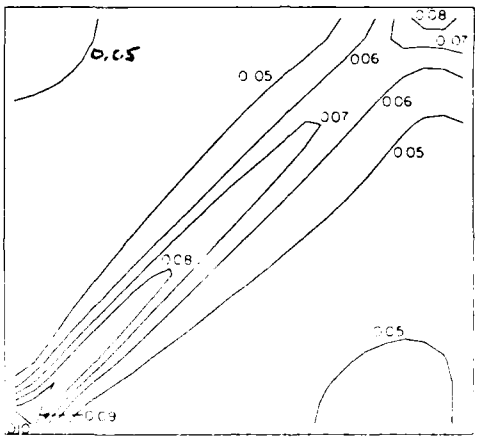

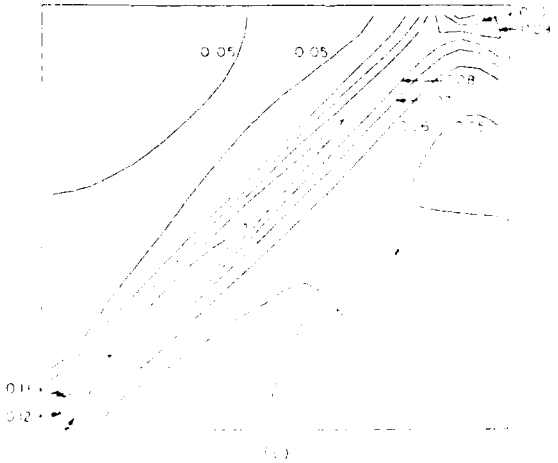

Figure 4

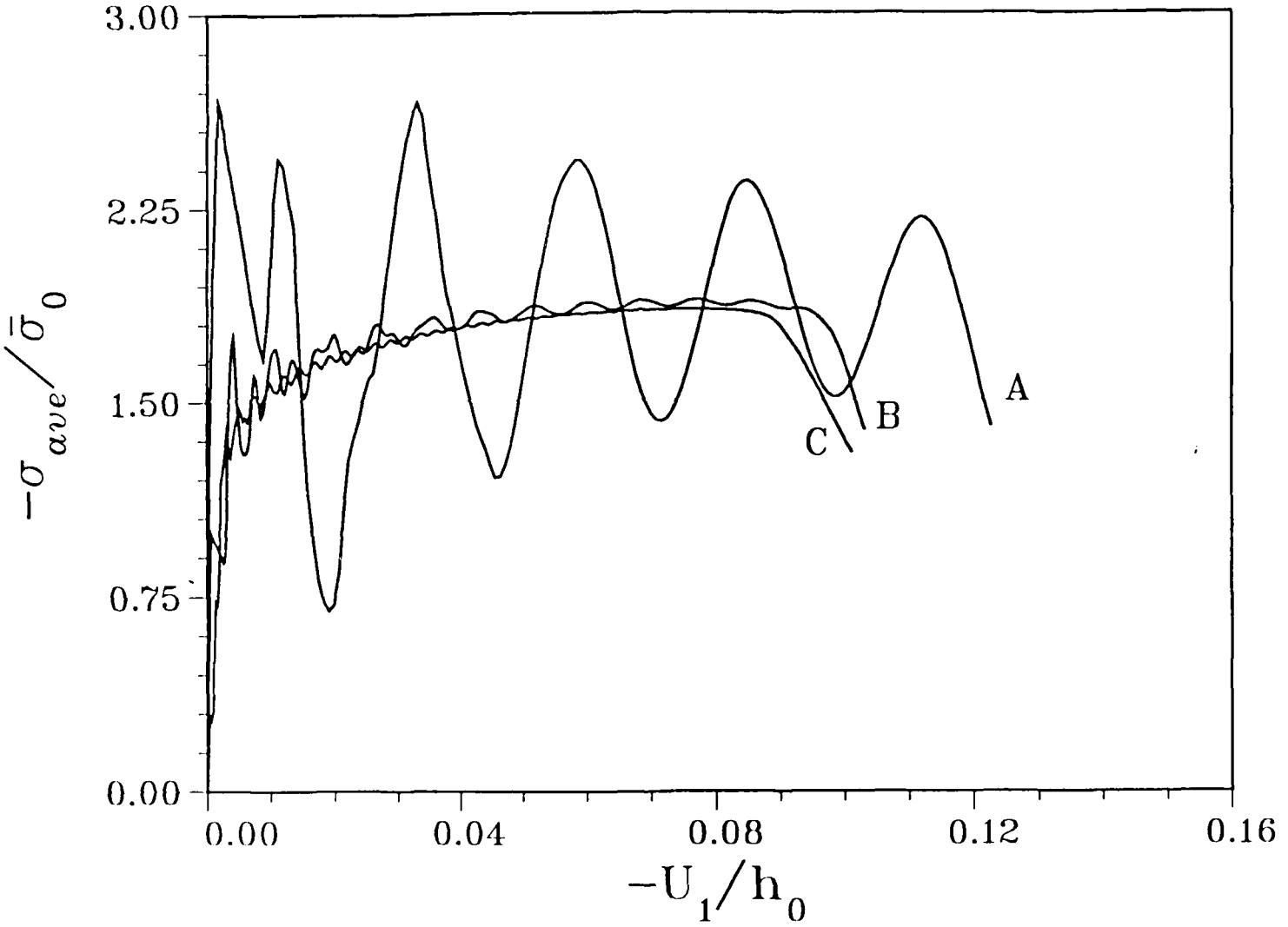
3.00
2.25
1.50
0.75
0.00
$-\sigma_{ave}/\bar{\sigma}_0$
0.00
0.04
0.08
0.12
0.16
$-U_1/h_0$
A
B
C

Figure 5

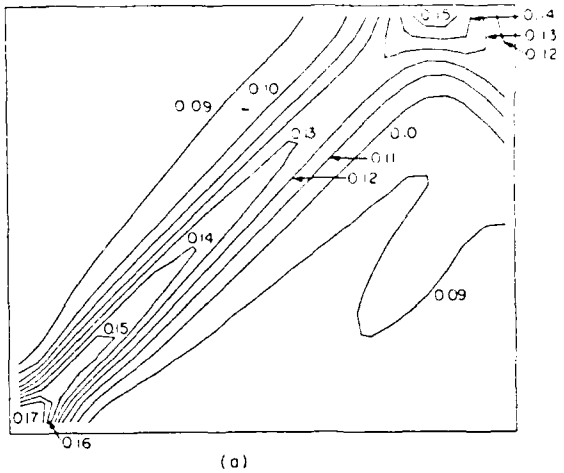
0.15
0.14
0.13
0.12
0.09
0.10
0.13
0.0
0.11
0.12
0.14
0.09
0.15
0.17
0.16

(a)

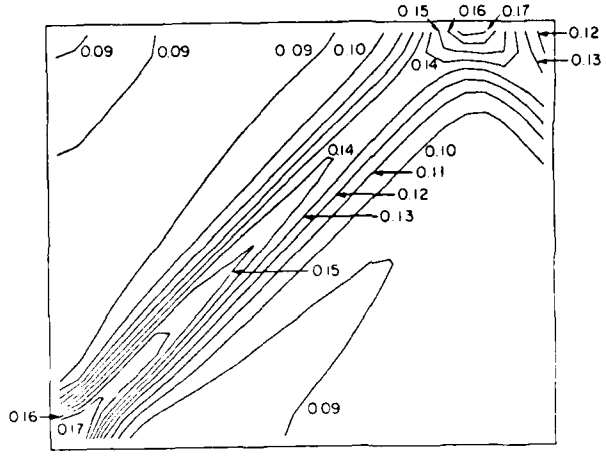
0.15
0.16
0.17
0.12
0.13
0.09
0.09
0.09
0.10
0.14
0.14
0.10
0.11
0.12
0.13
0.15
0.16
0.17
0.09

(b)

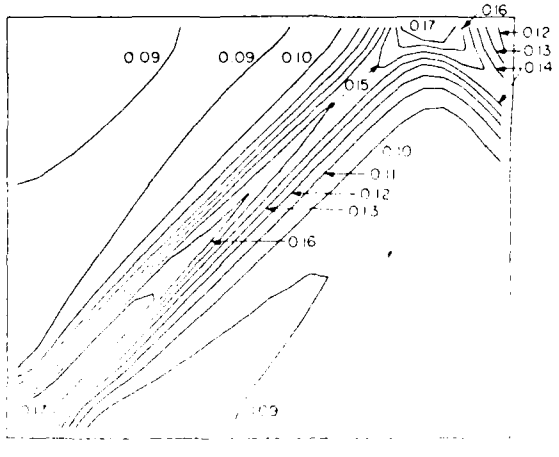
0.16
0.17
0.12
0.13
0.14
0.09
0.09
0.10
0.15
0.11
0.12
0.13
0.16

(c)

Figure 6

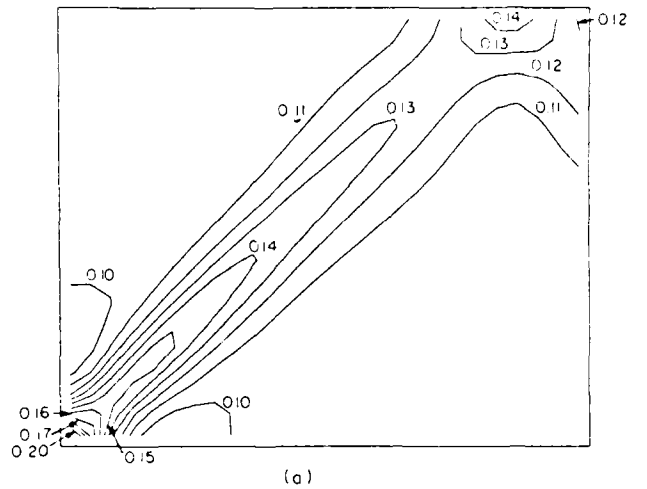
0.14
0.12
0.13
0.12
0.11
0.13
0.11
0.14
0.10
0.10
0.16
0.17
0.20
0.15

(a)

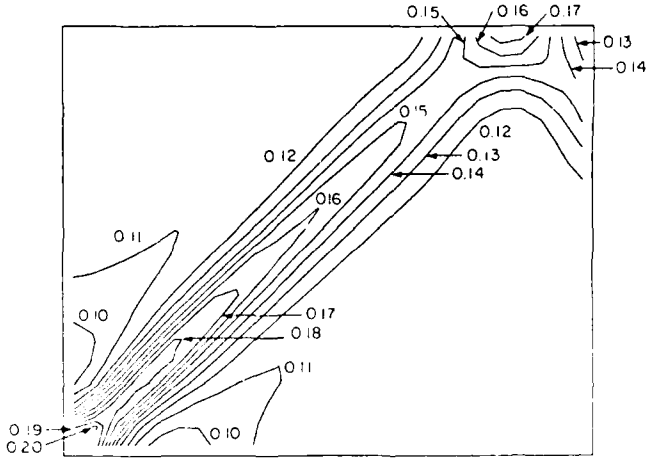
0.15
0.16
0.17
0.13
0.14
0.15
0.12
0.12
0.13
0.14
0.16
0.11
0.10
0.17
0.18
0.11
0.19
0.20
0.10

(b)

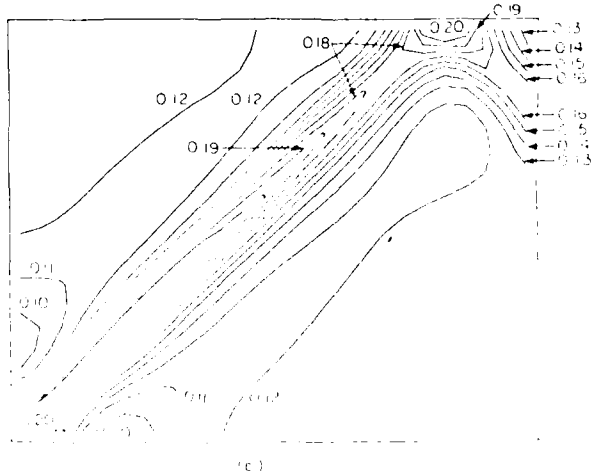
0.19
0.20
0.18
0.12
0.12
0.19

(c)

Figure 7

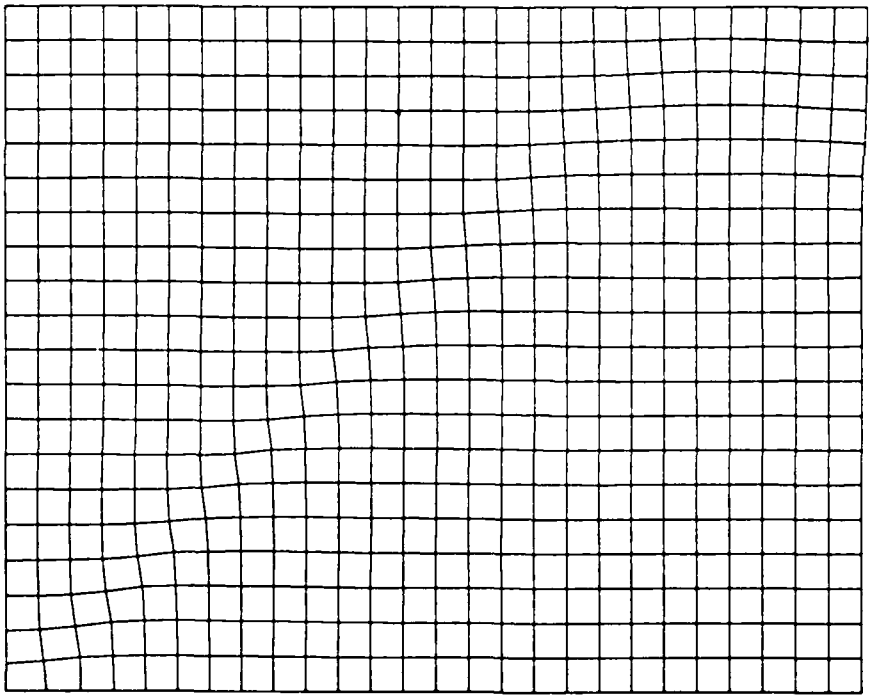

(a)

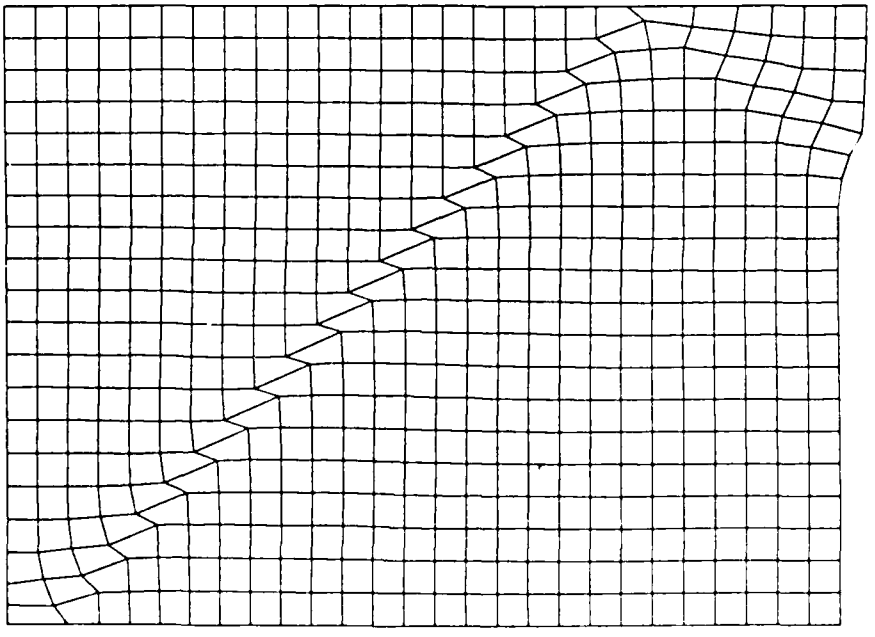

(b)

Figure 8

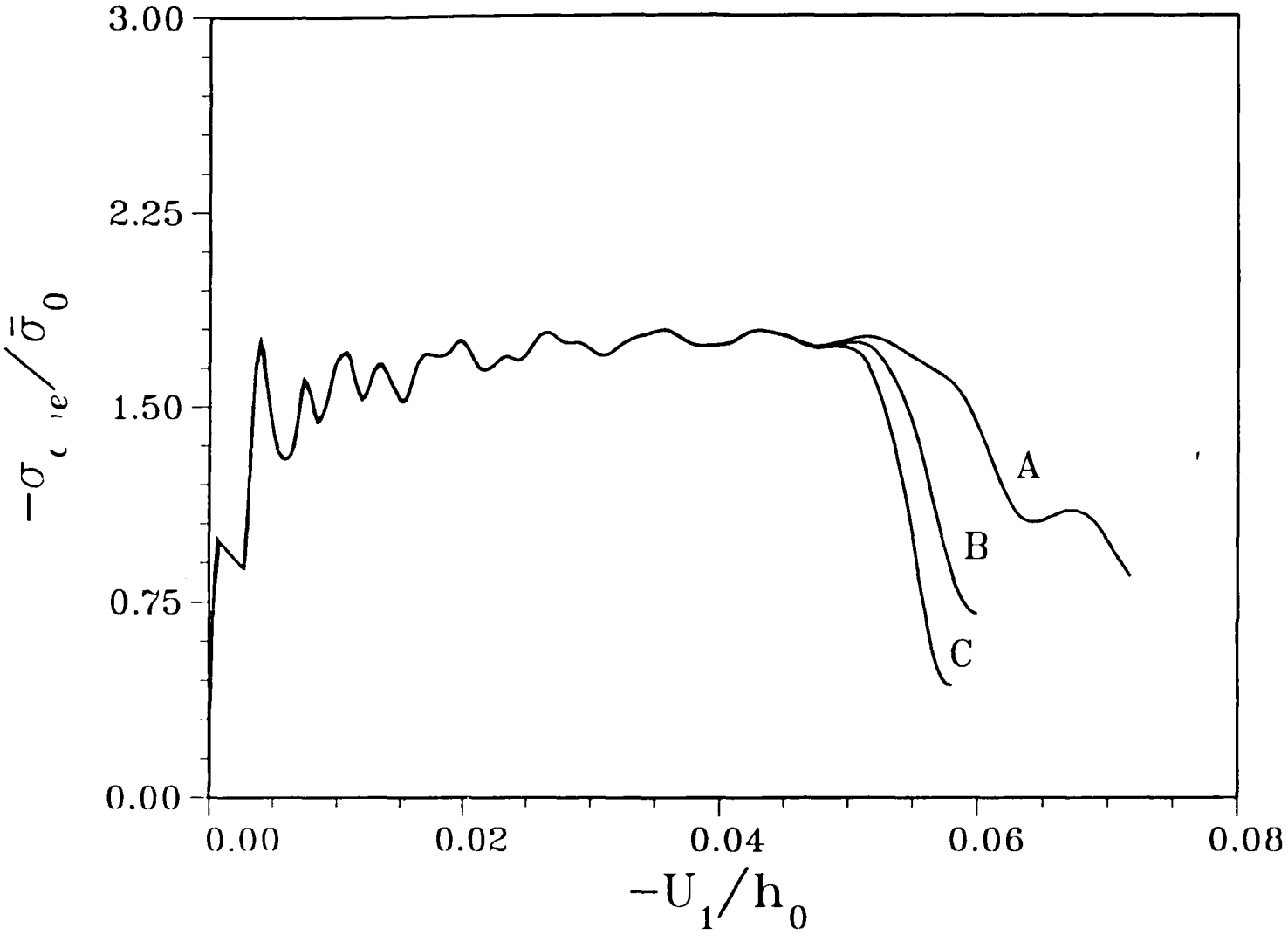
3.00
2.25
1.50
0.75
0.00
0.00
0.02
0.04
0.06
0.08
$-\sigma_{c\,re}/\bar{\sigma}_0$
$-U_1/h_0$
A
B
C

Figure 9

END

DATE

FILMED

5-88

DTIC